JOURNAL OF GEOPHYSICAL RESEARCH, VOL. 105, NO. A3, PAGES 5381–5389, MARCH 1, 2000

Precipitation of relativistic electrons by interaction with electromagnetic ion cyclotron waves

K. R. Lorentzen,[1] M. P. McCarthy, and G. K. Parks
Geophysics Program, University of Washington, Seattle

J. E. Foat,[2] R. M. Millan, D. M. Smith, and R. P. Lin
Space Sciences Laboratory, University of California, Berkeley

J. P. Treilhou
Centre d'Etude Spatiale des Rayonnements, Toulouse, France

Abstract. On August 20, 1996, balloon-borne X-ray detectors observed an intense X-ray event as part of a French balloon campaign near Kiruna, Sweden, at 1532 UT (1835 magnetic local time), on an L shell of 5.8. The energy spectrum of this event shows the presence of X rays with energies >1 MeV, which are best accounted for by atmospheric bremsstrahlung from monoenergetic ~1.7 MeV precipitating electrons. Ultraviolet images from the Polar satellite and energetic particle data from the Los Alamos geosynchronous satellites show the onset of a small magnetospheric substorm 24 min before the start of the relativistic electron precipitation event. Since the balloon was south of the auroral oval and there was no associated increase in relativistic electron flux at geosynchronous altitude, the event is interpreted as the result of selective precipitation of ambient relativistic electrons from the radiation belts. Pitch angle scattering caused by resonance with electromagnetic ion cyclotron mode waves is the most likely mechanism for selective precipitation of MeV electrons. A model is presented in which wave growth is driven by temperature anisotropies in the drifting substorm-injected proton population. The model predicts that this wave growth and resonance with ~1.7 MeV electrons will occur preferentially in regions of density >10 cm^{-3}, such as inside the duskside plasmapause bulge or detached plasma regions. The model predictions are consistent with the location of the balloon, the observed energies, and the timing with respect to the substorm energetic particle injection.

1. Introduction

Using a variety of techniques, relativistic electron precipitation (REP) events have been observed for over 30 years. The first REP events were inferred from changes in the propagation of radio waves [*Bailey and Pomerantz*, 1965]. Relativistic electrons can affect the scattering path and propagation of radio waves by causing changes in the ionosphere at altitudes below 70-75 km. Later, balloon-borne X-ray detectors were used to observe REP events. Electron precipitation creates X rays through the process of atmospheric bremsstrahlung, and balloon instruments at stratospheric altitudes can detect these X rays. *Rosenberg et al.* [1972] observed an REP event with an *e*-folding energy of 100–150 keV, and *West and Parks* [1984] observed an REP event with an *e*-folding energy of 200 keV. The type of X-ray detector used on these early balloon flights did not have the energy range or resolution to distinguish monoenergetic peaks of MeV energies from hard exponentially falling spectra. Satellite observations of REP events, such as those made by *Imhof et al.* [1986, 1991, 1997], *Nakamura et al.* [1995], and *Blake et al.* [1996], have the advantage of providing direct measurements of the precipitating electrons but have the disadvantage of being unable to observe for long periods of time and being unable to separate temporal and spatial effects.

Because of limitations in these measurement techniques, the processes causing the precipitation of relativistic electrons have not yet been adequately explained. Studying the mechanisms involved in the acceleration of these particles can further our understanding of energy transport between different regions of the magnetosphere. Improving our knowledge about these processes is also important for several practical reasons. Electrons of MeV energies can damage spacecraft [*Baker et al.*, 1986]. These electrons

[1] Now at The Aerospace Corporation, Los Angeles, California.

[2] Now at Green Institute of Geophysics and Planetary Physics, University of California, San Diego.

Paper number 1999JA000283.
0148-0227/00/1999JA000283$09.00

can also penetrate to altitudes of 40–70 km in the atmosphere, where they may dissociate molecules that can affect the ozone layer [*Callis et al.*, 1991].

Two different mechanisms have been proposed to account for the precipitation of MeV electrons from the radiation belts. Some nightside REP events have been attributed to the loss of adiabatic motion that occurs when the magnetic field line radius of curvature is small compared to an electron gyroradius [*Sergeev and Tsyganenko*, 1982; *Sergeev et al.*, 1983]. This mechanism acts near the nightside trapping boundary, where the magnetic field lines are stretched and have a smaller radius of curvature. Since the gyroradius increases with particle energy, this mechanism acts selectively on higher-energy particles such as MeV electrons. However, this mechanism cannot account for duskside REP events occurring in localized regions for moderately short periods.

The other mechanism that has been proposed to account for REP events, wave-particle interactions, is the focus of this paper. Electrons gyrating in a magnetic field can exchange energy with circularly polarized wave modes through cyclotron resonance, causing pitch angle scattering and electron precipitation. This mechanism has been shown to cause REP events over a range of wide range of L shells and local times [*Thorne and Andreoli*, 1980]. Several different wave modes can resonate with electrons, including the whistler and electromagnetic ion cyclotron (EMIC) wave modes.

In this paper we discuss balloon observations of a duskside MeV X-ray burst and related satellite observations of associated substorm activity. The X rays were observed by a set of instruments that provided both spatial and temporal information as well as a higher energy range and resolution than were used for previous balloon observations of REP events. A detailed description of the balloon observations has been presented elsewhere [*Foat et al.*, 1998]. The main purpose of this paper is to present a wave-particle interaction model that accounts for the balloon observations and relates them to the preceding substorm.

2. Observations

The balloon data used in this study were collected as part of the Interball and Balloon Observations of Aurora (INTERBOA) campaign in 1996. The balloon X-ray instruments included an X-ray imaging camera (XRI), which used a pinhole collimator to focus X rays onto a sodium iodide scintillator and a liquid nitrogen cooled germanium X-ray detector (GeD). The design of the XRI is described in detail by *Lorentzen* [1999]. Both instruments viewed a 45° half-angle vertical cone. The XRI measured X rays in the range 20–120 keV with an energy resolution of ~10 keV full width at half maximum (FWHM) at 60 keV, and the GeD measured X rays in the range 20–1400 keV with ~2 keV FWHM resolution. Other instruments on the balloon included a broadband X-ray detector, VLF sensors, and triaxial electric and magnetic field sensors.

On August 20, 1996, the balloon-borne X-ray instruments observed an intense X-ray event near Kiruna, Sweden. The temporal structure of this event is shown by the X-ray imager count rate in Figure 1. The event consisted of seven bursts of ~60–90 s separated by ~100–200 s. Superposed on some of the peaks is a ~10–20 s periodicity (see also the fast Fourier transform analysis by *Foat et al.* [1998]). The event began at 1532 UT (1835 magnetic local time (MLT)) and lasted until 1555 UT. At this time, K_p was ~2, and the balloon was located on an L shell of 5.8, as determined using the *Tsyganenko* [1989] magnetic field model. Immediately following the event, count rates returned to the pre-event background level.

The high-resolution energy spectra taken by the GeD are described in detail by *Foat et al.* [1998] and are reproduced in Figure 2. At the bottom of Figure 2 is the background spectrum taken before the event. In the middle of Figure 2, crosses and diamonds show background-subtracted count spectra taken during the first and second halves of the REP event, respectively. Note that a significant flux

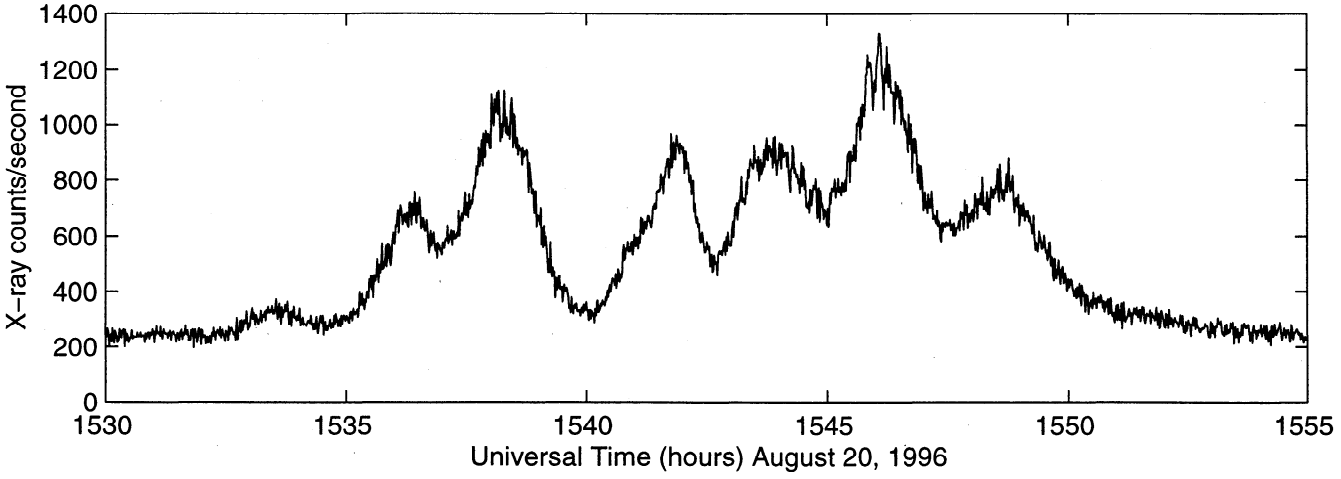

Figure 1. X-ray imager data taken during the relativistic electron precipitation event of August 20, 1996. The X-ray count rate between 20 and 120 keV is averaged over 1 s. The 10–20 s modulation is most clearly visible superposed on the peak starting near 1545 UT.

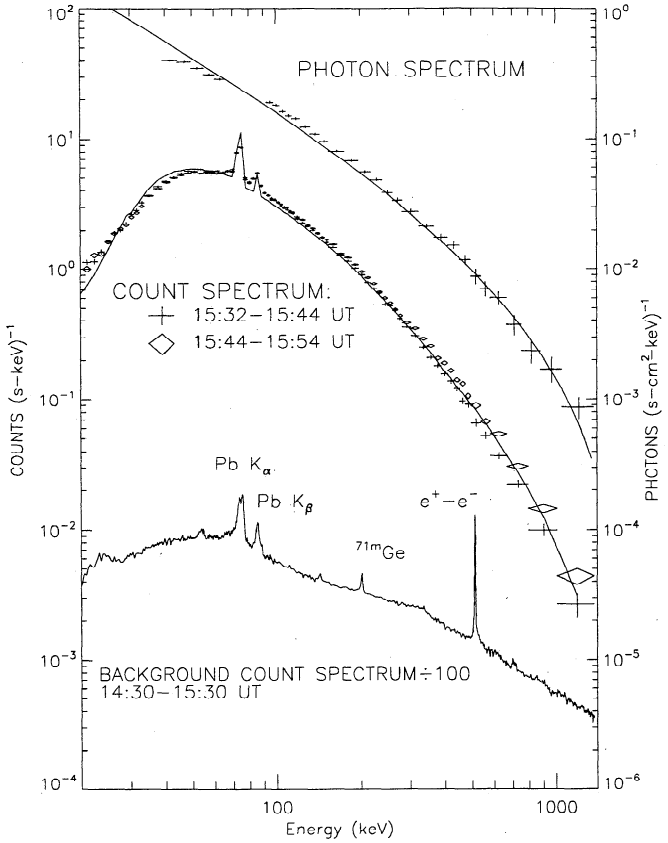

Figure 2. Data from the germanium detector (GeD) during the relativistic electron precipitation (REP) event, reproduced from *Foat et al.* [1998]. The bottom shows the background spectrum taken before the event. The crosses and diamonds in the middle show spectra measured on the balloon, and the crosses at the top show X-ray spectra corrected for instrument response and atmospheric absorption. The solid curves represent model calculations of X-ray spectra produced by monoenergetic 1.7 MeV precipitating electrons.

of X rays is visible up to the limit of the instrument at 1.4 MeV. At the top of Figure 2, crosses represent the photon spectrum corrected for the atmosphere and the instrument response. The solid lines in Figure 2 show model calculations of the X-ray spectra at the top of the atmosphere and at the instrument. The model calculations were made by assuming a form for the precipitating electron spectrum and using bremsstrahlung theory to calculate the X-ray spectrum produced. The best fit was obtained using an input spectrum consisting of monoenergetic ~1.7 MeV precipitating electrons. The exact shape of the monoenergetic electron peak cannot be determined, but the spectrum is dominated by electrons in the 1.5–2.0 MeV range, and the peak energy has an error of <0.2 MeV. The average electron precipitation was ~300 cm^{-2} s^{-1}, giving a flux of ~0.2–0.05 cm^{-2} s^{-1} sr^{-1} keV^{-1}, if we assume isotropic precipitation with a width in the range ~0.1–0.5 MeV. The spectra at peak and valley times were similar, although the event did show some hardening after 1544 UT.

Images from the XRI (not shown) indicate that the region of precipitation was larger than the field of view of the balloon instruments. No small-scale spatial structure was observed, and the region of precipitation brightened uniformly across the field of view, indicating that the seven bursts were a temporal feature, not a spatial feature. The penetration limit for 1–2 MeV electrons is <55 km altitude [*Berger and Seltzer*, 1972]. At these altitudes the field of view of the XRI and GeD would be < 50 km in diameter. These observations are consistent with observations by the imaging riometer for ionospheric studies (IRIS) in Kilpisjärvi, Finland. The imaging riometer recorded an ionospheric absorption feature of size ~200 (east–west) by ~100 km (north–south) at 90 km altitude (not shown), with temporal structure similar to the balloon X-ray observations. For absorption altitudes at ~60 km the feature would be ~160 by ~80 km, still larger than the field of view of the X-ray instruments.

An image from the Polar satellite ultraviolet imager (UVI) [*Torr et al.*, 1995] is shown in Figure 3. This image, along with others from the UVI, indicates the onset of a small magnetospheric substorm ~24 min before the start of the REP event. During the time of the REP event the substorm appeared to be in the recovery phase. The auroral oval remained well north of the balloon location during the entire period before and after the REP event.

Energetic particle data from the Los Alamos geosynchronous satellites [*Belian et al.*, 1992; *Meier et al.*, 1996] also indicate the onset of a small magnetospheric substorm ~24 min before the start of the relativistic electron precipitation event. Figure 4 shows these data (courtesy of Geoff Reeves at Los Alamos National Laboratory (LANL)). The proton injection in Figure 4b, 50–400 keV channels, shows only a slight dispersion, indicating that the spacecraft was west of, but very close to, the injection region, consistent with the UVI images.

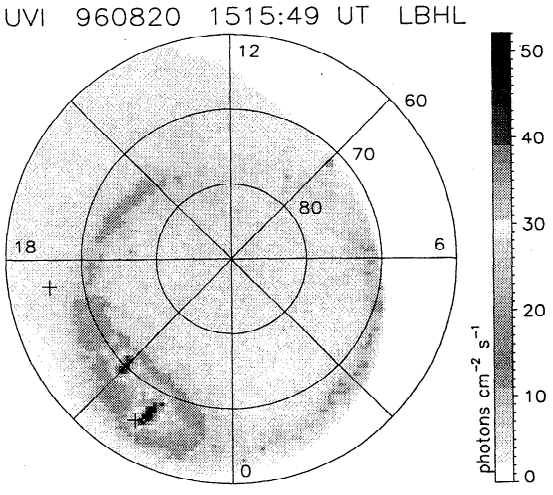

Figure 3. Polar ultraviolet image taken at 1516 UT, just after the substorm onset. The crosses show the position of the balloon (near dusk) and Los Alamos National Laboratory (LANL) satellite footprint (near 22 magnetic local time (MLT)).

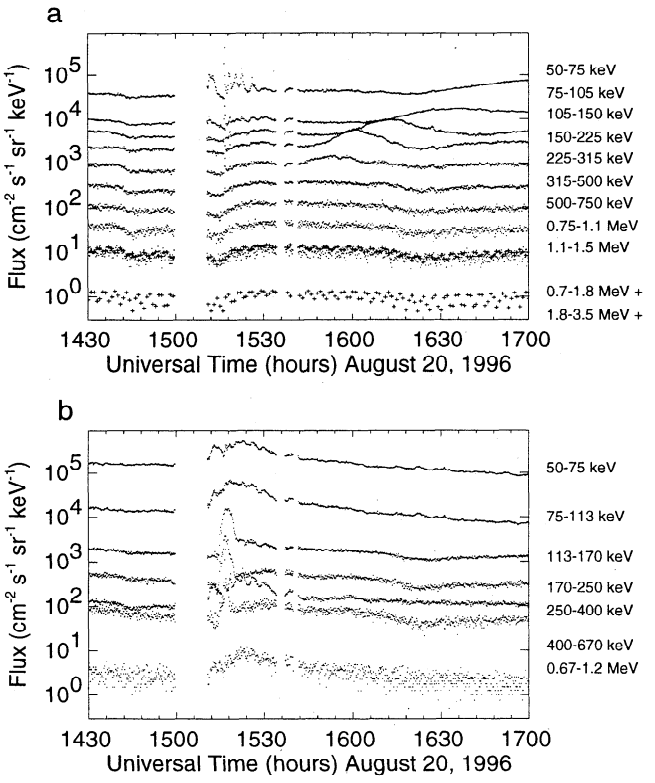

Figure 4. Energetic particle data from the Los Alamos geosynchronous satellite 1994-084. (a) Electron data marked by dots are from the synchronous orbit particle analyzer, and electron data marked with crosses are from the energetic spectrometer for particles. (b) Proton data are from the synchronous orbit particle analyzer. The 400–670 keV proton channel may be contaminated.

3. Modeling Relativistic Electron Precipitation

The position of the balloon with respect to the auroral oval suggests that electrons originated in the outer radiation belts. However, geosynchronous satellites observed no coincident increases in the flux of relativistic electrons. Therefore we interpret this event as the result of some mechanism selectively causing precipitation of ambient MeV electrons and not a mechanism causing acceleration of lower-energy electrons such as those described by *Li et al.* [1997] and *Baker et al.* [1994]. The trapped electron flux between 1.8 and 3.5 MeV is ~1 cm^{-2} s^{-1} sr^{-1} keV^{-1} (see Figure 4), which is well above the precipitating electron flux of ~0.2–0.05 cm^{-2} s^{-1} sr^{-1} keV^{-1} calculated from the balloon measurements. Even with uncertainties of a factor of 2 in these measurements, the ambient radiation belt population could easily supply the precipitating electrons.

Since wave-particle interactions are the most likely mechanism to account for the duskside REP events, we investigated wave-particle interactions with both whistler mode waves and with EMIC mode waves. These wave modes have been identified as most likely to interact with relativistic electrons [*Horne and Thorne*, 1998; *Summers et al.*, 1998]. We find that interaction with EMIC mode waves can best explain the observed energies, the duskside location, and the timing with respect to the substorm. In sections 3.1–3.3 we examine the effect of the substorm on the plasma population near the field line mapping to the balloon location, the energies of electrons interacting with different wave modes, and the parameters influencing the wave growth.

3.1. Drift of Substorm-Injected Particles

The bounce-averaged drift velocity can be determined from

$$V_D = 2.56 \times 10^6 \, (0.7 + 0.3 \sin \alpha) \, L \, \gamma m v^2, \qquad (1)$$

where V_D is the drift velocity in degrees per minute, α is the pitch angle on the equator, L is the magnetic L shell where the particles are located, γ is the relativistic mass factor, $1/\sqrt{1 - v^2/c^2}$, m is the particle mass, and v is the particle velocity [*Roederer*, 1970]. Equatorially mirroring particles correspond to the $\alpha \approx 90°$ case, and marginally trapped particles correspond to the $\alpha \approx 0°$ case. Electrons will drift to the east, and protons will drift to the west.

Figure 5 shows the time taken for electrons and protons to drift from the substorm injection longitude to the balloon longitude, as a function of energy. Figure 5 shows that at the time when the balloon began observing the REP event, 24 min after the substorm onset, 60 keV protons and 400 keV electrons would have drifted from the injection region to the region mapping to the balloon. However, the LANL satellite data shown in Figure 4 do not show any substorm features in the 400 keV electron flux, while there is a definite increase in the 60 keV proton flux. Therefore substorm-injected protons are more likely than electrons to play a role in the REP event.

Cornwall et al. [1970] suggested that ring current protons in this energy range are unstable to ion cyclotron wave

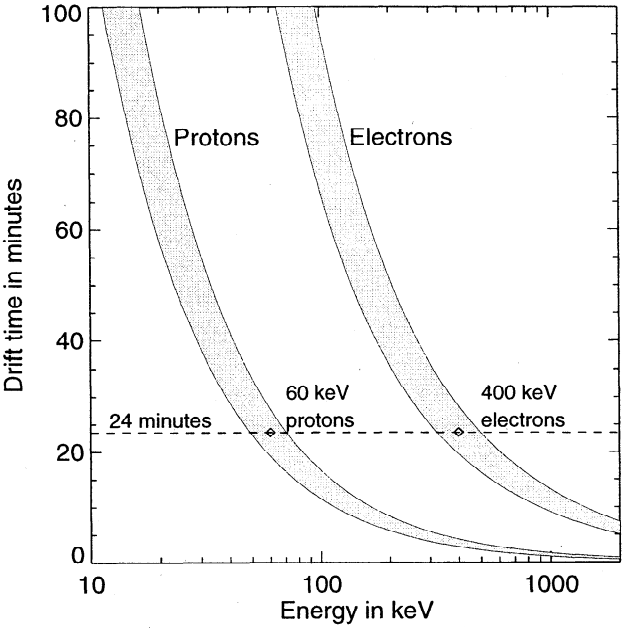

Figure 5. Gradient curvature drift times in minutes for particles drifting around the Earth at $L = 6$, from the LANL satellite 1991-084 at 175° magnetic longitude (near midnight) to the balloon field line at 118° magnetic longitude (near dusk). The shaded region of each curve gives the range of drift times for $\alpha \approx 0°$ to $\alpha \approx 90°$.

growth in the region just inside the plasmapause. *Thorne and Kennel* [1971] proposed that these waves could cause parasitic precipitation of relativistic electrons. Later, *Lyons and Thorne* [1972] and *Thorne* [1974] expanded upon this idea. A statistical study of the occurrence frequency of Pc 1–2 EMIC waves showed that although these waves occur most commonly for $L > 7$, they do occur predominantly in the afternoon sector in the $L = 6$–7 range [*Anderson et al.*, 1992]. Although the drift calculations indicate that the substorm is more likely to lead to ion instabilities than electron instabilities on the duskside, we examine both ion- and electron-driven waves for completeness.

3.2. Wave-Particle Interactions

Electrons can resonate with circularly polarized waves if the following resonance condition is satisfied:

$$\omega - k_{\|} v_{\|} = s\Omega_e/\gamma. \tag{2}$$

Here ω is the wave frequency, $k_{\|}$ is the wave number parallel to the magnetic field, $v_{\|}$ is the component of the electron velocity parallel to the magnetic field, s is an integer (positive for resonance with right-hand circularly polarized whistler mode waves and negative for anomalous resonance with left-hand circularly polarized EMIC mode waves), and Ω_e is the unsigned electron gyrofrequency, $|q_e|B/m_e c$, with q_e the charge on the electron and B the magnetic field strength. If this resonance condition is satisfied, waves and particles can exchange energy, causing pitch angle scattering and precipitation.

Whistler mode waves are right-hand circularly polarized waves whose cold-plasma dispersion relation for parallel propagation is given by

$$n^2 = \frac{c^2k^2}{\omega^2} = \frac{\omega_{pe}^2}{\omega(\Omega_e - \omega)}, \tag{3}$$

where n is the index of refraction, k is the wave number, and ω_{pe} is the electron plasma frequency, $\sqrt{4\pi N_e q_e^2/m_e}$, and N_e is the electron number density [*Kennel and Petschek*, 1966]. This dispersion relation is valid for $\Omega_i \ll \omega < \Omega_e \ll \omega_{pe}$, where Ω_i is the ion gyrofrequency.

Combining this dispersion relation with the relativistic electron resonance condition from (2) for $s = +1$ and solving for v allows us to determine the energy of the resonant electrons. For nonrelativistic electrons, there is a single solution for $v_{\|}$. However, for highly relativistic electrons, the factor of γ introduces $v_{\perp}$ into the resonance condition, giving a range of solutions for $v_{\|}$.

By assuming $\gamma \approx 1$, *Thorne and Andreoli* [1980] obtained

$$\frac{E_{\rm res}}{m_e c^2} = \left[\frac{2E_{\rm mag}}{m_e c^2}\frac{\Omega_e}{\omega}\left(1 - \frac{\omega}{\Omega_e}\right)^3 + 1\right]^{1/2} - 1, \tag{4}$$

where $E_{\rm res}$ is the resonant electron kinetic energy in the parallel direction ($v_{\perp}/c \ll 1$) given by $m_e c^2(\gamma - 1)$ and $E_{\rm mag} = B^2/8\pi N$ is the magnetic energy per particle with N being the total plasma density.

For electron energies near 2 MeV, γ is close to 5, so the low-gamma approximation given in (4) overestimates the value of E_{res}. However, the approximation does provide a way to examine easily the form of the function. The resonant electron energy depends on three factors: the magnetic field strength, the wave frequency, and the plasma density. Figure 6 shows the relation between resonant electron energy and whistler mode wave frequency for various equatorial plasma densities at $L = 6$. Figure 6 shows that whistler resonance with electrons of ~1.7 MeV can only occur for low plasma densities and low wave frequencies. Since whistler mode waves are not usually observed on the equator at frequencies below 0.1 Ω_e [*Tsurutani and Smith*, 1977], this wave mode is unlikely to account for our observations. Therefore we look next at the EMIC mode wave.

Electromagnetic ion cyclotron waves are left-hand circularly polarized waves whose cold-plasma dispersion relation for parallel propagation, assuming $\omega < \Omega_i \ll \omega_{pi}$ [*Kennel and Petschek*, 1966], is given by

$$n^2 = \frac{c^2k^2}{\omega^2} = \frac{\omega_{pi}^2}{\Omega_i(\Omega_i - \omega)}, \tag{5}$$

where ω_{pi} is the ion plasma frequency, $\sqrt{4\pi N_i q_i^2/m_i}$, N_i is the ion number density, q_i is the ion charge, m_i is the mass of an ion, and Ω_i is the unsigned ion cyclotron frequency, $|q_i|B/m_i c$.

Combining the EMIC dispersion relation with the relativistic electron resonance condition given in (2) for $s = -1$ and using $\omega \ll \Omega_e$ (reasonable for the EMIC mode since $\omega < \Omega_i = \Omega_e/1836$), we can obtain a formula for $E_{\rm res}$, the parallel electron kinetic energy that is resonant with the waves [*Thorne and Andreoli*, 1980]. No approximations for γ are used in this derivation.

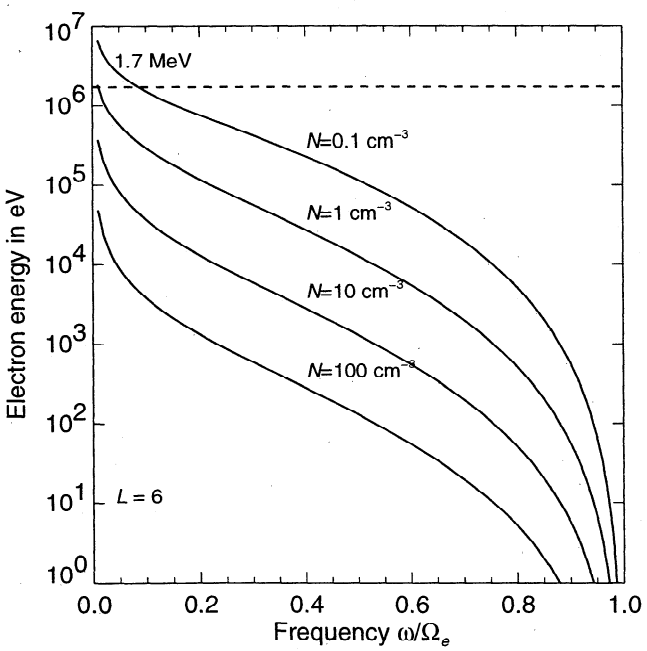

Figure 6. Electron parallel resonance energy for various plasma densities and whistler wave frequencies calculated using the low-gamma approximation from (4).

$$\frac{E_{\rm res}}{m_e c^2} = \left[\frac{2E_{\rm mag}}{m_e c^2}\left(\frac{m_i}{m_e}\right)\left(\frac{\Omega_i}{\omega}\right)^2\left(1-\frac{\omega}{\Omega_i}\right)+1\right]^{1/2} - 1. \quad (6)$$

Figure 7 shows the relation between resonant electron energy and EMIC mode wave frequency for various equatorial plasma densities at $L = 6$. Figure 7 shows that EMIC resonance with electrons of ~1.7 MeV is most likely to occur for plasma densities above 10 cm^{-3}. These densities are reasonable for regions inside the plasmasphere or in detached plasma regions. Since our observations were made on the duskside during quiet geomagnetic conditions, it is not unlikely that the plasmasphere extended beyond $L = 6$ at this time. In addition, proton densities of ~50 cm^{-3} were measured by the magnetospheric plasma analyzer [*Bame et al.*, 1993] on the LANL geosynchronous satellite 1990-095, which passed through the duskside region 5 hours after the REP event was observed.

From these simple calculations we conclude that interaction of relativistic electrons with EMIC mode waves provides a feasible mechanism for the selective precipitation of radiation belt electrons near dusk. EMIC mode waves can more reasonably account for the observed X-ray energies than whistler mode waves. We next turn our attention to studying the growth of EMIC mode waves in order to constrain further the likelihood of this mechanism as an explanation for the August 20, 1996, event.

3.3. Growth of Electromagnetic Ion Cyclotron Mode Waves

We have no direct observations of waves associated with this REP event. In order to determine whether wave-particle interactions can account for our observations we need to assess whether conditions are favorable for the growth of waves at the desired mode and frequency.

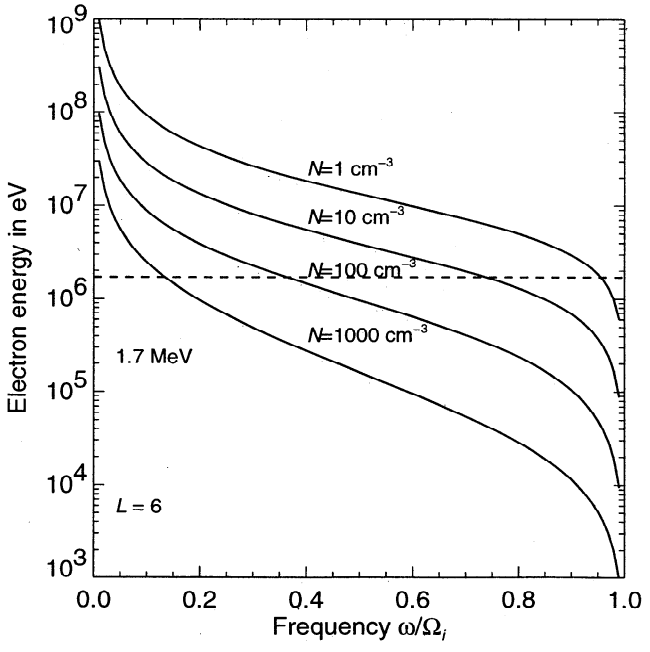

Figure 7. Electron parallel resonance energy for various plasma densities and electromagnetic ion cyclotron (EMIC) wave frequencies calculated using (6).

A complex dispersion relation for EMIC mode waves in a plasma with bi-Maxwellian components can be obtained from Maxwell's equations and the Vlasov equation [*Stix*, 1992; *Melrose*, 1986]. We examined a plasma consisting of cold isotropic electrons, cold isotropic ions, and warm anisotropic ions. These components represent the cold background plasma with the addition of warm substorm-injected ions. For the case of parallel-propagating EMIC mode waves in such a plasma, the following dispersion relation is obtained:

$$\frac{c^2k^2}{\omega^2} \approx 1 - \frac{\omega_{pce}^2}{(\omega^2-\Omega_e^2)} - \frac{\omega_{pci}^2}{(\omega^2-\Omega_i^2)} + \frac{\omega_{pwi}^2}{\omega^2}A - \frac{\omega_{pwi}^2}{\omega^2}\left\{\frac{\zeta_{+1}Z(\zeta_{+1})}{2}\left[\frac{\omega}{(\omega-\Omega_i)}+A\right] + \frac{\zeta_{-1}Z(\zeta_{-1})}{2}\left[\frac{\omega}{(\omega+\Omega_i)}+A\right]\right\} \quad (7)$$

where the subscripts c and w refer to the cold and warm components, respectively, A is the temperature anisotropy, $T_\perp/T_\parallel - 1$, and Z is the plasma dispersion function [*Stix*, 1992],

$$Z(\zeta_s) = \frac{1}{\sqrt{\pi}}\int_{-\infty}^{\infty}\frac{e^{-z^2}}{z-\zeta_s}\,dz, \quad (8)$$

$$\zeta_s = \frac{(\omega - s\Omega_{wi})}{\sqrt{2}k_\parallel V_{Twi\parallel}}. \quad (9)$$

By numerically solving this dispersion relation for ω we can determine at what frequencies wave growth will occur. Wave growth will occur at frequencies where the imaginary part of ω is greater than zero. The frequency at which ions are most unstable to wave growth can then be used in (6) to determine the energies of the resonant electrons.

Equation (7) involves five free parameters: the magnetic field strength, the cold ion density, the warm ion density, the warm ion temperature, and the warm ion temperature anisotropy. We do not have direct measurements of all of these quantities, so we varied the parameters to determine a model plasma that can account for our observations. Table 1 gives the range of parameters studied. Each one of these five parameters was varied while keeping the other four constant in order to find the dependence of the model on these variables.

Figure 8 shows the variation of the wave frequency and electron resonant energy with cold ion density, N_{ci}. Figure 8a shows that the wave frequency at which growth is maximum decreases as the cold ion density increases. However, Figure 8b shows that the corresponding electron resonant energy does not show much change with density, except at cold ion densities below 10 cm^{-3}. Above this density the line for resonant electron energy is quite flat. This result was somewhat surprising. Equation (6) says that the electron resonant energy is inversely dependent on cold ion density (through the magnetic energy, $B^2/8\pi N$). However, the electron resonant energy is also inversely dependent on the wave frequency, which is, in turn, inversely dependent on the cold ion density. The interrelationship of these values results in an electron resonant energy independent of cold ion density above ~10 cm^{-3}. For the remaining calculations a

Table 1. Free Parameters in the Model

	Range		
Magnetic field strength, nT	50	–	350
Cold ion density, cm^{-3}	1	–	1000
Warm ion density, cm^{-3}	0.01	–	1
Warm ion energy, keV	5	–	90
Warm ion anisotropy	0.5	–	13

value of 50 cm^{-3} was used since that matched the LANL satellite observation made later at the same local time.

The model sensitivity to variation in magnetic field strength was found to be <10 keV per nT. The scale size of the event was ~100 km, which corresponds to ~0.5 in L value or ~30 nT, assuming a dipole field. Since the duskside magnetosphere is reasonably well approximated by a dipole field during moderately quiet periods, a value of 144 nT, corresponding to $L = 6$, is used in the model.

The remaining three free parameters all correspond to the drifting warm substorm-injected ions. This population changes rapidly as it drifts, and the only in situ measurements are from the LANL satellite located at the injection point. From these measurements, and using a simple drift simulation such as is described by *Solomon* [1975] and *Lin and Parks* [1976], the warm ion density and average energy were calculated for a drifting Maxwellian population. No measurements were available for the temperature anisotropy of the warm substorm-injected ions, but the drift simulation was used to constrain a reasonable range of values.

Each of these three warm ion parameters could significantly affect the resonant electron energy, so the combined effects of all three parameters are summarized in Figure 9. Figure 9 shows the range of warm ion parameters that would be needed to interact with 1.7 MeV electrons in a region where the magnetic field strength was 144 nT and the cold plasma density was 50 cm^{-3}. In order to produce waves that will interact with 1.7 MeV electrons, high densities, low average energies, or high temperature anisotropies are needed. Other parameters result in waves that would interact only with electrons of energies of the order of 10 MeV.

Uncertainties in the position and width of the substorm injection region imply that almost any density and average energy shown in Figure 9 might reasonably represent the injected population. Although the temperature anisotropies are high, they represent only the anisotropy in the warm ion component, a small percentage of the total plasma population. Hence this model demonstrates that EMIC mode waves driven by drifting substorm-injected protons can reasonably account for the REP event observed by the balloon-borne instruments.

4. Discussion

Figure 10 gives a cartoon representation of the model. Figure 10 illustrates the three main parts of the model: the drift of substorm-injected protons, the growth of ion cyclotron mode waves inside the high-density plasmasphere, and the selective precipitation of MeV electrons by pitch angle scattering inside the high-density plasmasphere.

This model explains the energies of the balloon X-ray observations, their location and restricted spatial scale, as well as their association with the coincident substorm. The size of the precipitation region is of the order of 100 km. Mapping this region to the equator gives a size of ~1500 km at $L = 6$. Since this length is only a fraction of the size of the typical plasmapause bulge, it is most likely that the electron precipitation originated in a small detached plasma region. This scale size is similar to that inferred from satellite motion across bands of electron precipitation by *Nakamura*

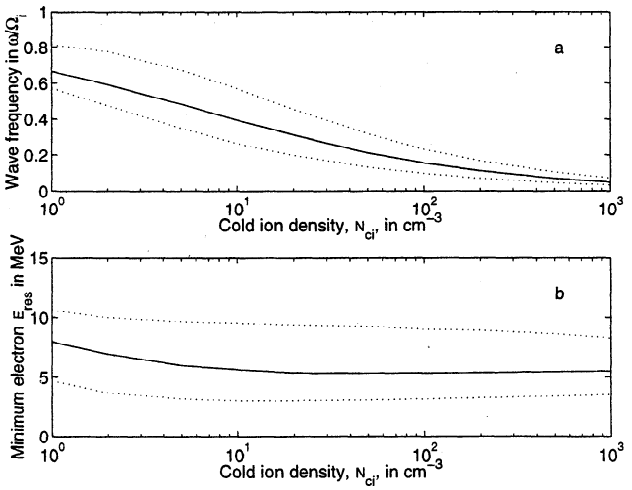

Figure 8. Variation of cold ion density with $B = 140$ nT, $N_{wi} = 0.11$ cm^{-3}, $E_{avg} = 45$ keV, and $A_{wi} = 4.6$: (a) wave frequency versus cold ion density and (b) electron resonant energy versus cold ion density. The solid line shows the value corresponding to maximum wave growth, and the dotted lines show the range of positive wave growth.

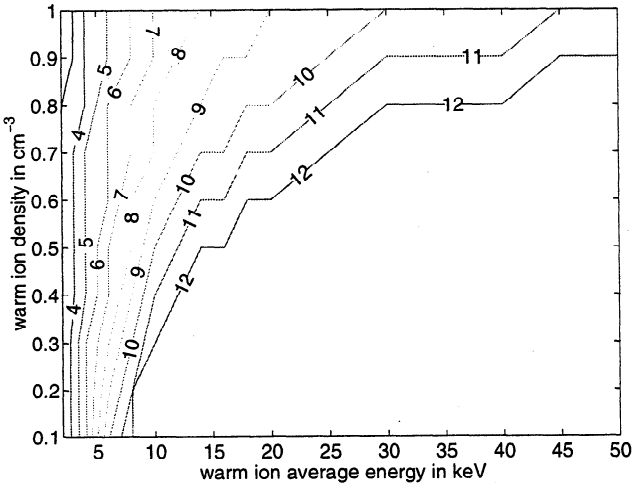

Figure 9. The contours show the temperature anisotropy $(T_\perp/T_\parallel - 1)$ needed to produce waves that will interact with 1.7 MeV electrons, for various combinations of warm ion density and energy. The magnetic field strength was chosen to correspond to $L = 6$, and the cold ion density was 50 cm^{-3}.

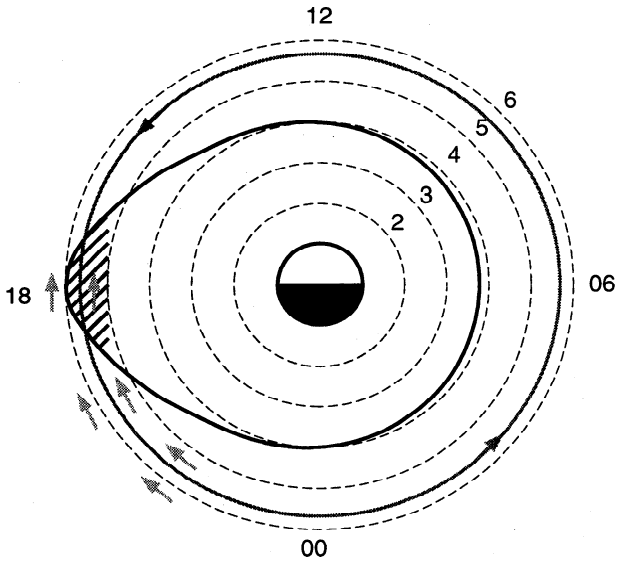

Figure 10. A cartoon explanation of the duskside REP model, after *Thorne and Kennel* [1971]. The egg-shaped region represents an idealized plasmapause. The short arrows show the drift of substorm-injected protons toward dusk. The hatched region inside the plasmapause represents the region where electromagnetic ion cyclotron wave growth is driven. The solid circle shows the approximate direction of drift of ambient relativistic electrons in the radiation belts. These electrons are present at all local times but interact with ion cyclotron waves only in the hatched region inside the plasmapause.

et al. [1995] and *Blake et al.* [1996], suggesting that these events may be caused by similar phenomena.

Future work will involve attempting to explain the complicated temporal structure observed in the X-ray bursts. Several potential explanations have been examined, but we are unable to account for the dramatic variations in count rate seen on a timescale of several minutes nor for the ~10–20 s periodicity superposed on some of the peaks.

One conceivable explanation for the presence of the seven large amplitude bursts is the similarity of this temporal structure to that seen in the substorm-injected proton population. However, a simulation of the drift of this proton distribution from the nightside to the duskside indicates that this temporal structure would be smoothed out by the time the protons had drifted over to the field line mapping to the balloon.

An alternate explanation for this low-frequency modulation may be a relationship to a field line resonance that was observed at the same time as the X-ray bursts [*Foat et al.*, 1998]. This field line resonance had several frequency components, including one that was close to the ~150 s period of the X-ray bursts. A field line resonance could modulate the wave growth proposed in the present model in such a way as to modulate the pitch angle scattering and precipitation of the electrons. However, as described in section 3, changes in the magnetic field strength would also lead to changes in the resonant energy of the electrons. Such changes in the energy spectra of the precipitating electrons between the minima and maxima are inconsistent with observations.

It was suggested by *Foat et al.* [1998] that the 10–20 s periodicity seen in the X-ray count rate could be the frequency of the ion cyclotron wave resonant with the electrons. However, on the basis of this assumption they found that the required densities were much higher than typical plasmaspheric values and concluded that EMIC mode waves could not account for the observations. However, it is likely that the frequency of the X-ray modulations does not actually represent the EMIC mode wave frequency since the mechanism pitch angle scatters the electrons independent of the wave phase. For an L shell of 6 this periodicity corresponds to 0.025-0.050 times the equatorial ion gyrofrequency and is only observed during part of the REP event. Another mechanism, such as modulation of the EMIC wave growth, may be responsible for producing this periodicity. More work is needed to explain the temporal features of this event.

Another important point is that the model considers only hydrogen ions in the EMIC growth rate calculations. However, helium ions may also play an important role. Although helium is probably not present in significant enough quantities to drive the wave growth, small quantities of helium ions can introduce stop bands in the frequency spectrum driven by hydrogen ions [*Kozyra et al.*, 1984]. These stop bands are located at 0.25 Ω_{H+} and can change the EMIC mode wave spectra, influencing the energies of relativistic electrons precipitated. However, we do not have enough data from the August 20, 1996, REP event to test a more complicated multiple ion simulation.

While there are several steps that could be taken to improve the model explaining this event, we lack sufficient data to test such theories. Future work on this type of duskside relativistic electron precipitation event will depend on further observations. Observations from stationary balloon platforms are ideal for this kind of study since they can provide detailed information on the spectral characteristics of the precipitation while at the same time resolving spatial and temporal ambiguities. However, the most valuable information will result from the correlation of balloon observation with ground and satellite observations. Combining balloon observations with satellite observations of waves and particles on field lines mapping to the balloon location would provide the best means for testing whether interaction with EMIC mode waves can account for other duskside REP events.

Acknowledgments. The imaging riometer for ionospheric studies (IRIS) is operated by the Communications Research Centre at Lancaster University, United Kingdom, funded by the Particle Physics and Astronomy Research Council (PPARC) in collaboration with Sodankylä Geophysical University. LANL energetic particle data were provided by Geoff Reeves. LANL magnetospheric plasma analyzer data were obtained from the D. McComas at the CDA web site. The research at the University of Washington and the University of California, Berkeley, was supported by NSF grant ATM 9223612 in 1996-1997. In 1998, UW was supported by NSF grant ATM 9806400 and UCB was supported by NASA grant NAG5-6870. The research at CESR was supported by CNES grant 96CNES208 and the balloon campaign was managed by CNES. One of the authors (K.R.L.) was supported by a NASA Graduate Student Researchers Fellowship. We thank John Chin and

Tim Chinowsky at UW and Greg Zimmer at UCB for electronics support. We also thank Mitch Brittnacher at UW for producing the UVI images.

Janet G. Luhmann thanks Daniel Baker for his assistance in evaluating this paper.

References

Anderson, B. J., R. E. Erlandson, and L. J. Zanetti, A statistical study of Pc 1-2 magnetic pulsations in the equatorial magnetosphere, 1, Equatorial occurrence distributions, *J. Geophys. Res.*, *97*, 3075, 1992.

Bailey, D. K., and M. A. Pomerantz, Relativistic electron precipitation into the mesosphere at subauroral latitudes, *J. Geophys. Res.*, *70*, 5823, 1965.

Baker, D. N., J. B. Blake, R. W. Klebesadel, and P. R. Higbie, Highly relativistic electrons in the Earth's outer magnetosphere, 1, Lifetimes and temporal history 1979-84, *J. Geophys. Res.*, *91*, 4265, 1986.

Baker, D. N., J. B. Blake, L. B. Callis, J. R. Cummings, D. Hovestadt, S. Kanekal, B. Klecker, R. A. Mewaldt, and R. D. Zwickl, Relativistic electron acceleration and decay time scales in the inner and outer radiation belts: SAMPEX, *Geophys. Res. Lett.*, *21*, 409, 1994.

Bame, S. J., et al., Magnetospheric plasma analyzer for spacecraft with constrained resources, *Rev. Sci. Instrum.*, *64*, 1026, 1993.

Belian, R. D., G. R. Gisler, T. Cayton, and R. Christensen, High-Z energetic particles at geosynchronous orbit during the great solar proton event series of October 1989, *J. Geophys. Res.*, *97*, 16,897, 1992.

Berger, M. J., and S. M. Seltzer, Bremsstrahlung in the atmosphere, *J. Atmos. Terr. Phys.*, *34*, 85, 1972.

Blake, J. B., M. D. Looper, D. N. Baker, R. Nakamura, B. Klecker, and D. Hovestadt, New high temporal and spatial resolution measurements by SAMPEX of the precipitation of relativistic electrons, *Adv. Space Res.*, *18* (8), 171, 1996.

Callis, L. B., D. N. Baker, J. B. Blake, J. D. Lambeth, R. E. Boughner, M. Natarajan, R. W. Klebesadel, and D. J. Gorney, Precipitating relativistic electrons: Their long-term effect on stratospheric odd nitrogen levels, *J. Geophys. Res.*, *96*, 2939, 1991.

Cornwall, J. M., F. V. Coroniti, and R. M. Thorne, Turbulent loss of ring current protons, *J. Geophys. Res.*, *75*, 4699, 1970.

Foat, J. E., et al., First detection of a terrestrial MeV X-ray burst, *Geophys. Res. Lett.*, *25*, 4109, 1998.

Horne, R. B., and R. M. Thorne, Potential waves for relativistic electron scattering and stochastic acceleration during magnetic storms, *Geophys. Res. Lett.*, *25*, 3011, 1998.

Imhof, W. L., H. D. Voss, D. W. Datlowe, E. E. Gaines, J. Mobilia, and D. S. Evans, Relativistic electron and energetic ion precipitation spikes near the plasmapause, *J. Geophys. Res.*, *91*, 3077, 1986.

Imhof, W. L., H. D. Voss, J. Mobilia, D. W. Datlowe, and E. E. Gaines, The precipitation of relativistic electrons near the trapping boundary, *J. Geophys. Res.*, *96*, 5619, 1991.

Imhof, W. L., D. L. Chennete, E. E. Gaines, and J. D. Winningham, Characteristics of electrons at the trapping boundary of the radiation belt, *J. Geophys. Res.*, *102*, 95, 1997.

Kennel, C. F., and H. E. Petschek, Limit on stably trapped particle fluxes, *J. Geophys. Res.*, *71*, 1, 1966.

Kozyra, J. U., T. E. Cravens, A. F. Nagy, E. G. Fontheim, and R. S. B. Ong, Effects of energetic heavy ions on electromagnetic ion cyclotron wave generation in the plasmapause region, *J. Geophys. Res.*, *89*, 2217, 1984.

Li, X., et al., Multisatellite observations of the outer zone electron variation during the November 3-4, 1993, magnetic storm, *J. Geophys. Res.*, *102*, 14,123, 1997.

Lin, C. S., and G. K. Parks, Ion cyclotron instability of drifting plasma clouds, *J. Geophys. Res.*, *81*, 3919, 1976.

Lorentzen, K. R., Duskside relativistic electron precipitation, Ph.D. thesis, Univ. of Wash., Seattle, 1999.

Lyons, L. R., and R. M. Thorne, Parasitic pitch angle diffusion of radiation belt particles by ion cyclotron waves, *J. Geophys. Res.*, *77*, 5608, 1972.

Meier, M., R. Belian, T. Cayton, R. Christensen, B. Garcia, K. Grace, J. Ingraham, J. Laros, and G. Reeves, The energy spectrometer for particles (ESP): Instrument description and orbital performance, in *Workshop on the Earth's Trapped Particle Environment*, edited by G. Reeves, p. 203, Am. Inst. of Phys., College Park, Md, 1996.

Melrose, D. B., *Instabilities in Space and Laboratory Plasmas*, Cambridge Univ., New York, 1986.

Nakamura, R., D. N. Baker, J. B. Blake, S. Kanekal, B. Klecher, and D. Hovestadt, Relativistic electron precipitation enhancements near the outer edge of the radiation belt, *Geophys. Res. Lett.*, *22*, 1129, 1995.

Roederer, J. G., *Dynamics of Geomagnetically Trapped Radiation*, Springer-Verlag, New York, 1970.

Rosenberg, T. J., L. J. Lanzerotti, D. K. Bailey, and J. D. Pierson, Energy spectra in relativistic electron precipitation events, *J. Atmos. Terr. Phys.*, *34*, 1977, 1972.

Sergeev, V. A., and N. A. Tsyganenko, Energetic particle losses and trapping boundaries as deduced from calculations with a realistic magnetic field model, *Planet. Space Sci.*, *30*, 999, 1982.

Sergeev, V. A., E. M. Sazhina, N. A. Tsyganenko, J. Å. Lundblad, and F. Søraas, Pitch-angle scattering of energetic protons in the magnetotail current sheet as the dominant source of their isotropic precipitation into the nightside ionosphere, *Planet. Space Sci.*, *31*, 1147, 1983.

Solomon, J., Drift of particles and wave-particle interactions, in *The Magnetospheres of the Earth and Jupiter*, edited by V. Formisano, p. 153, D. Reidel, Norwell, Mass., 1975.

Stix, T. H., *Waves in Plasmas*, Am. Inst. of Phys., College Park, Md., 1992.

Summers, D., R. M. Thorne, and F. Xiao, Relativistic theory of wave-particle resonant diffusion with application to electron acceleration in the magnetosphere, *J. Geophys. Res.*, *103*, 20,487, 1998.

Thorne, R. M., A possible cause of dayside relativistic electron precipitation events, *J. Atmos. Terr. Phys.*, *36*, 635, 1974.

Thorne, R. M., and L. J. Andreoli, Mechanisms for intense relativistic electron precipitation, in *Exploration of the Polar Upper Atmosphere*, edited by C. S. Deehr and J. A. Holtet, p. 381, D. Reidel, Norwell, Mass., 1980.

Thorne, R. M., and C. F. Kennel, Relativistic electron precipitation during magnetic storm main phase, *J. Geophys. Res.*, *76*, 4446, 1971.

Torr, M. R., et al., A far ultraviolet imager for the international solar-terrestrial physics mission, *Space Sci. Rev.*, *71*, 329, 1995.

Tsurutani, B. T., and E. J. Smith, Two types of magnetospheric ELF chorus and their substorm dependencies, *J. Geophys. Res.*, *82*, 5112, 1977.

Tsyganenko, N. A., A magnetospheric magnetic field model with a warped tail current sheet, *Planet. Space Sci.*, *37*, 5, 1989.

West, R. H., and G. K. Parks, ELF emissions and relativistic electron precipitation, *J. Geophys. Res.*, *89*, 159, 1984.

J. E. Foat, Green Institute of Geophysics and Planetary Physics, University of California, San Diego, CA 92093-0255

R. P. Lin, R. M. Millan, and D. M. Smith, Space Sciences Laboratory, University of California, Berkeley, CA 94720-7450.

K. R. Lorentzen, The Aerospace Corporation, P. O. Box 92957, Los Angeles, CA 90009-2957. (kirsten.r.lorentzen@aero.org)

M. P. McCarthy and G. K. Parks, Geophysics Program, University of Washington, Seattle, WA 98195-1650.

J. P. Treilhou, Centre d'Etude Spatiales des Rayonnements, 9, avenue du Colonel Roche, 31400 Toulouse, France.

(Received August 5, 1999; revised November 10, 1999; accepted November 22, 1999.)